Influence of Loop Shortening on the Metal Binding Site of Cupredoxin Pseudoazurin[†,‡]

Milko Velarde,[§] Robert Huber,[§] Sachiko Yanagisawa,[||] Christopher Dennison,*[,||] and Albrecht Messerschmidt*[,§]

Abteilung Proteomics und Signaltransduktion, Max-Planck-Institut für Biochemie, Am Klopferspitz 18, 82152 Martinsried, Germany, and Institute for Cell and Molecular Biosciences, Medical School, Newcastle University, Newcastle upon Tyne NE2 4HH, United Kingdom

Received June 6, 2007; Revised Manuscript Received June 11, 2007

ABSTRACT: Atomic resolution structures of the pseudoazurin (PAZ) variant into which the shorter ligand-containing loop of amicyanin (AMI) is introduced have been determined. The mutated loop adopts a different conformation in PAZAMI than in AMI. The copper site structure is affected, with the major influence being an increased axial interaction resulting in the shortest Cu(II)−S(Met) bond observed for the cupredoxin family of electron-transfer proteins. This is accompanied by a lengthening of the important Cu−S(Cys) bond and enhanced tetragonal distortion, consistent with the influence of the PAZAMI loop contraction on the UV/vis spectrum. The change in active site geometry is the major cause of the 50 mV decrease in reduction potential. The copper site structure changes very little upon reduction, consistent with the distorted site still possessing the properties required to facilitate rapid electron transfer. The exposed His ligand on the loop protonates in the reduced protein and reasons for the increased pK_a compared to that of PAZ are discussed. The area surrounding the His ligand is more hydrophobic in PAZAMI than in PAZ, while electron self-exchange, which involves homodimer formation via this surface patch, is decreased. The nature of the side chains in this region, as dictated by the sequence of the ligand-containing loop, is a more significant factor than hydrophobicity for facilitating transient protein interactions in PAZ. The structure of PAZAMI demonstrates the importance of loop−scaffold interactions for metal sites in proteins.

The small blue copper proteins (cupredoxins) have molecular weights of approximately 10 to 14 kDa and consist of a single β-barrel domain with a Greek-key fold. These proteins function as electron transfer (ET[1]) shuttles and contain a type 1 (T1) copper site with peculiar spectroscopic properties (*1*). Cupredoxin domains also occur in a range of enzymes including the copper-containing nitrite reductases (NiRs) and the multi-copper oxidases (*1*−*3*). The four canonical T1 copper ligands are a His, donated from a β-strand in the core of the fold, and Cys, His, and usually Met on the loop linking the C-terminal strands of the β-barrel (Figure 1). This site appears perfectly adapted to its function because the geometry is a compromise between those preferred by Cu(II) and Cu(I) (*4*, *5*), and there is very little change upon redox interconversion (*1*, *4*). The protein scaffold is thought to constrain the metal site and therefore facilitate rapid ET (*4*). However, theoretical studies have questioned this role of the cupredoxin domain in minimizing the inner-sphere reorganization energy (λ_i) (*5*−*8*). The

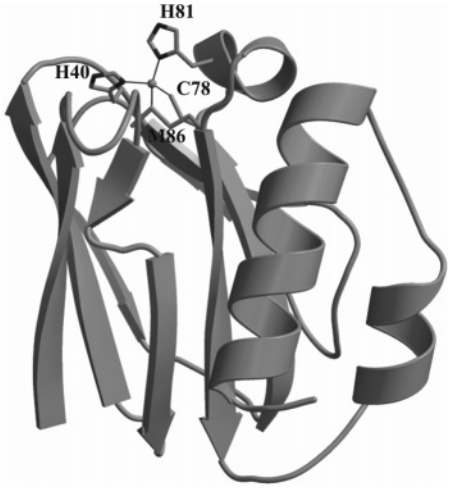

FIGURE 1: Ribbon representation of the structure of Cu(II) PAZ (1BQK; pH 6.0; (*17*)). The ligating residues are displayed as stick models and are labeled, and the copper ion is represented by a sphere.

* To whom correspondence should be addressed. Tel: +49 89 8578 2669. Fax: +49 89 8578 2219. E-mail: messersc@biochem.mpg.de (A.M.). Tel: +44 191 222 7127. Fax: +44 191 222 7424. E-mail: Christopher.dennison@ncl.ac.uk (C.D.).

† BBSRC (BB/C504519), Universities UK (ORS award to S.Y.), and Newcastle University are acknowledged for supporting this work.

‡ Coordinates for the structures described in this article have been deposited in the Protein Data Bank with codes 2UX6, 2UX7, 2UXF, and 2UXG.

§ Max-Planck-Institut für Biochemie.

|| Newcastle University.

[1] Abbreviations: ET, electron transfer; T1, type 1; λ_i, inner-sphere reorganization energy; AMI, amicyanin; AZ, azurin; PAZ, pseudoazurin; PC, plastocyanin; WT, wild type; AZAMI, azurin chimera in which the amicyanin loop has been introduced; AZPC, azurin chimera in which the plastocyanin loop has been introduced; PAZAMI, pseudoazurin chimera in which the amicyanin loop has been introduced; E_m, reduction potential; ESE, electron self exchange; k_{ESE}, electron self exchange rate constant; rmsd, root mean square deviation; ESU, estimated standard uncertainty.

10.1021/bi701113w CCC: $37.00
Published on Web 08/09/2007

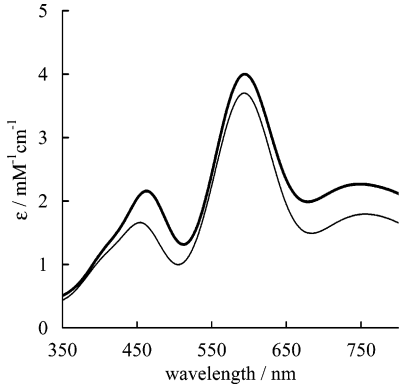

FIGURE 2: UV/vis spectra of PAZ (thin line) and PAZAMI (thick line) at 25 °C in 10 mM phosphate buffer at pH 8.0.

C-terminal metal binding loop has different lengths in cupredoxin domains and ranges from 7 to 15 amino acid residues. These proteins therefore provide a suitable system for investigating the importance of loop length and structure for the active-site integrity of a metalloprotein, and loop-directed mutagenesis has been used to investigate the role of this important region (*9*−*16*).

The consequences of introducing the shortest C-terminal T1 copper binding loop (that with the sequence CTPHPFM from amicyanin, AMI) into the β-barrel scaffolds of azurin (AZ), pseudoazurin (PAZ), and plastocyanin (PC), all with longer naturally occurring active site loops has been studied (*11*−*15*). The resulting loop-contraction variants possess T1 copper centers and are redox active. The structure of the AZ mutant (AZAMI) demonstrates that its active site is very similar to that of the wild type (WT) protein (*15*). The introduced AMI loop adopts a conformation almost identical to that found in the native protein. A similar outcome is obtained when the PC loop is introduced into AZ (*16*). The AZAMI mutation lowers the reduction potential (E_m) of AZ to that of AMI *(12*), while the AZPC variant has an E_m value 100 mV higher than that of AZ, which matches that of PC (*16*). These studies demonstrate that the structure of the active-site loop is a key feature for controlling this physiologically important parameter in cupredoxins.

All of the structures of chimeric cupredoxins that have been determined to date have utilized the AZ scaffold (*15*, *16*). In order to assess the influence of the scaffold onto which the loop is grafted, it is essential to have structural information on chimeras based on other cupredoxins. PAZAMI (the PAZ variant in which the $C^{78}TPH^{81}YGMGM^{86}$ loop has been replaced with the $C^{78}TPH^{81}P^{82}F^{83}M^{84}$ sequence of AMI) (*11*, *12*) provides the ideal option as the PAZ scaffold (see Figure 1), is distinct from that of AZ (PAZ is therefore a misnomer for this protein), and is unique among the cupredoxins in possessing a C-terminal extension consisting of two α-helices that pack onto the surface of the β-barrel, one of which interacts with the copper-binding loop (*17*). The PAZAMI mutation influences the UV/vis spectrum of the Cu(II) protein (see Figure 2) and lowers E_m by ∼50 mV (*11*, *12*). The pK_a value for the C-terminal His81 ligand, which protonates and dissociates in the Cu(I) protein, a feature that occurs in certain cupredoxins and is thought to have a physiological regulatory role (*18*−*21*), is raised by 2 pH units to 6.7 in PAZAMI to match the value for AMI (*11*, *12*). The intrinsic ET reactivity, measured using the electron self-exchange (ESE) rate constant (k_{ESE}), is 8-fold lower in PAZAMI than in PAZ. These changes are the most significant of the cupredoxin variants in which the AMI loop has been introduced (*11*, *12*). The crystal structures of the Cu(II) and Cu(I) forms of PAZAMI have been determined at two pH values to facilitate understanding of these effects and highlight that loop−scaffold interactions can have a significant influence on the active-site structure of a cupredoxin.

EXPERIMENTAL PROCEDURES

Cloning, Expression, and Purification of PAZAMI. The plasmid pTrcPazAmi harboring the gene for PAZAMI (*Achromobacter cycloclastes* PAZ variant in which the C-terminal ligand-containing loop of *Paracoccus versutus* AMI has been introduced) (*11*, *12*) was expressed in *Escherichia coli* BL21 cells. Cell growth, protein isolation, and purification were performed as described previously (*11*, *12*), except that prior to the first extraction step using carboxymethyl (CM) sepharose (GE Healthcare) the protein was dialyzed against 30 mM Tris at pH 6.5 containing 500 μM $Cu(NO_3)_2$.

Crystallization, Data Collection, and Structure Determination. Crystals of PAZAMI were obtained by the hanging drop vapor diffusion method mixing 1 μL of protein (20 mg/mL in 50 mM Tris at pH 7.5 plus 30 mM NaCl) with 1 μL of reservoir solution (10 mM Tris pH 7.5 plus 2 M ammonium sulfate and 2 M NaCl). Blue oxidized crystals of PAZAMI were reduced by adding 50 mM mercaptoethanol to the reservoir solution (the crystals became colorless after ∼3 h). X-ray diffraction data sets were collected at the DESY beamline BW6 at 100 K after transferring the crystals into a cryo-protectant solution (made by adding 25% glycerol to the reservoir solution). A MarCCD165 detector (Mar Research, Norderstedt, Germany) was used, and the wavelength for data collection was 1.05 Å. Two data sets of the same crystal of Cu(II) PAZAMI were collected, the first one at a crystal to detector distance that allowed an evaluation to 1.35 Å. The second data set could be integrated to the full resolution of 1.30 Å. Both data sets revealed data collection statistics in the same range (details for the lower resolution data are not shown). The crystal remained blue throughout the collection of both data sets indicating that reduction of the metal site by the X-ray photons had not occurred. The space group was determined as *R*32 with $a = 105.63$ Å, $b = 105.63$ Å, $c = 57.93$ Å, $\alpha = \beta = 90°$, and $\gamma = 120°$. Data sets from two different reduced crystals were obtained with resolutions of 1.30 Å and 1.35 Å with slightly altered cell constants of $a = 105.76$ Å, $b = 105.76$ Å, $c = 57.28$ Å (space group *R*32). These two data sets of Cu(I) PAZAMI were collected to check the estimated precision of the structures determined in this work, and particularly that of the copper site geometry.

Crystals were obtained for Cu(II) PAZAMI at pH 5.5 also using the hanging drop vapor diffusion method mixing 1 μL of protein (20 mg/mL in 100 mM Mes at pH 5.5 and 30 mM NaCl) with 1 μL of reservoir solution (100 mM Mes at pH 5.5, 2 M ammonium sulfate, and 2 M NaCl). After cryo-protection, a data set was acquired at 100 K on a Mar345 Image Plate system (Mar Research, Norderstedt, Germany) mounted on a rotating anode generator (MSC

Table 1: Crystallographic Data Collection and Refinement Statistics

	Cu(II) PAZAMI, pH 7.5	Cu(I) PAZAMI, pH 7.5	Cu(II) PAZAMI, pH 5.5	Cu(I) PAZAMI, pH 5.5
		data collection[a]		
wavelength, Å	1.050	1.050	1.542	1.542
space group	*R*32	*R*32	*R*32	*R*32
resolution range, Å	50.0−1.30 (1.35−1.30)	50.0−1.30 (1.35−1.30)	50.0−2.00 (2.07−2.00)	50.0−1.98 (2.05−1.98)
unit cell parameters, Å	$a = b = 105.63$, $c = 57.93$	$a = b = 105.76$, $c = 57.28$	$a = b = 105.57$, $c = 57.29$	$a = b = 105.36$, $c = 56.49$
no. of unique reflections	28824 (2149)	29429 (2780)	8274 (775)	8140 (541)
redundancy	3.6 (3.2)	15.2 (11.7)	4.2 (3.5)	7.1 (3.8)
$I/\sigma(I)$	14.3 (3.1)	15.7 (3.6)	23.3 (6.3)	18.5 (2.8)
completeness, %	94.5 (71.4)	97.6 (94.0)	98.6 (94.4)	95.6 (64.3)
R_{merge},[b] %	6.4 (29.0)	9.4 (39.1)	5.6 (18.6)	5.7 (22.0)
		refinement[a]		
resolution, Å	20.0−1.30 (1.33−1.30)	30.0−1.30 (1.34−1.30)	30.0−2.00 (2.05−2.00)	30.0−1.99 (2.04−1.99)
R_{factor},[c] %	19.5 (23.8)	19.2 (23.6)	16.6 (19.8)	16.3 (19.3)
R_{free}, %, test set 5%	22.6 (29.4)	20.1 (21.8)	20.4 (20.8)	23.0 (30.2)
rmsd bond lengths, Å	0.010	0.008	0.017	0.016
total number of atoms	1023	1026	991	1018
rmsd bond angles, °	1.2	1.2	1.5	1.6
Av. *B*-factor (protein, Å^2)	25.6	18.1	38.7	40.0
Av. *B*-factor (water, Å^2)	30.9	30.0	40.0	43.8
B-factor (Cu, Å^2)	23.8	25.2	36.3	65.9
rmsd bonded *B*'s[d]	1.4	1.4	1.8	2.0
ESU based on R_{factor}, Å	0.057	0.053	0.171	0.175
ESU based on R_{free}, Å	0.061	0.052	0.149	0.171
ESU based on maximum likelihood, Å	0.043	0.032	0.103	0.107

[a] The figures in parantheses represent data for the highest-resolution shell (as given). [b] $R_{merge} = \Sigma(I - \langle I \rangle)/\Sigma I$. [c] $R_{factor} = \Sigma(|F_{obs}| - |F_{calc}|)/\Sigma|F_{obs}|$. [d] The root-mean-square deviation of bonded *B*-factors is a measure of the smoothness of the *B*-factor refinement.

Rigaku, the Woodlands, TX) operated at 5.4 kW ($\lambda = CuK_\alpha = 1.5418$ Å). The crystal was still blue after data collection. The reduced form was prepared as described above, and the crystal, which was completely colorless after 3 h, was cryoprotected and a data set collected at 100 K. Data evaluation for all intensity sets was performed with the program HKL2000 (*22*) and revealed R_{merge} values below 0.10 with completeness values of better than 94%. Detailed data collection statistics are shown in Table 1.

The crystal structure of the Cu(II) PAZAMI at pH 7.5 was solved by molecular replacement with the program MOLREP (*23*) using the structure of PAZ from *A. cycloclastes* (PDB code 1BQK) (*17*) as a search model. Solvent molecules, the ligand-containing loop (residues 78−86), and the copper ion were omitted to avoid model bias. MOLREP delivered a prominent solution, which was subjected to a first round of crystallographic refinement with REFMAC5 (*24*). The corresponding $2F_o-F_c$ and F_o-F_c maps showed clear electron density for the missing polypeptide loop and the copper ion. Model building of the loop and all subsequent model building were performed with the program O (*25*). For the other structures, the refined model of the pH 7.5 Cu(II) form without the copper ion and solvent molecules was used for an initial rigid body refinement with REFMAC5. Water molecules were generated with the automated Arp/Warp procedure available in REFMAC5 when run with the CCP4i user interface (*26*). In all structures, one glycerol molecule and one Cl^- ion were identified. All other crystallographic refinements were performed in REFMAC5. Some residues show electron density due to alternate main chain or side chain conformations, which were incorporated in the refinement. Because of the high resolution of all of the structures, copper site geometries have been refined without any constraints. The crystallographic refinement converged in all cases giving satisfactory *R*-values, and detailed refinement statistics are listed in Table 1. The stereochemistry of the models was analyzed with PROCHECK (*27*). For the superimposition of structures, the program LSQMAN (*28*) was used. The solvent accessibility of active sites was calculated with SurfRace using a probe radius of 1.4 Å (*29*). Figures of protein structures were prepared with BOBSCRIPT (*30*) and Raster3D (*31*). The coordinates and structure factors have been submitted to the Protein Data Bank with PDB ID codes 2UX6 [Cu(II) PAZAMI, pH 7.5], 2UX7 [Cu(I) PAZAMI, pH 7.5], 2UXF [Cu(II) PAZAMI, pH 5.5], and 2UXG [Cu(II) PAZAMI, pH 5.5].

RESULTS

Overall Structures. All of the PAZAMI structures are very similar and retain the overall fold of the scaffold protein PAZ (*17*) with an 8-stranded β-barrel and a 30 residue C-terminal extension consisting of two α-helices that pack onto the surface of the β-barrel (see Figure 3). The first helix is small (~1.5 turns), while the more C-terminal helix consists of

FIGURE 3: Superimposed ribbon representations of the structures of Cu(II) PAZ at pH 6.0 (1BQK in green (*17*)) and PAZAMI at pH 7.5 (blue). The ligating residues and the side chain of Phe83 are displayed as stick models and are labeled, and the copper ion is represented by a gray sphere for PAZAMI.

approximately four turns. The conformation of the main chain fold was checked with a Ramachandran plot calculated with PROCHECK. In all cases, 91.9% of the residues lie in the most favored regions and the remaining 8.1% in additionally allowed areas. The PAZAMI structures superimpose with root-mean-square deviations (rmsds) below 0.15 Å for the C^{α} atoms of residues 1−9, 16−50, and 53−122. (The loops between residues 10 and 15 and 51 and 52 have been omitted from this comparison because they display disorder in the Cu(II) structure at pH 7.5 and have been modeled with two main chain conformations.) Certain Met and Lys residues show electron density for alternate side chain conformations that have been modeled. The rmsd for the superimposition of the C^{α} atoms of residues 1−9, 16−50, 53−78, and 85−122 of PAZAMI with the corresponding amino acids of PAZ (PDB code 1BQK) (*17*) is 0.94 Å. This relatively high value is partly due to movement of the C-terminal α-helix (residues 91−122), which arises from the positioning of the phenyl ring of Phe83 close to the first turn of this region (see Figure 3). Furthermore, in PAZAMI, a glycerol molecule binds between the Phe68 to Val73 loop and the Gly52 to Phe56 region via a number of hydrogen-bonding contacts. These interactions result in backbone alterations in these regions compared to PAZ. The crystal packing in the PAZAMI structure is different from that for PAZ, resulting in adjacent molecules interacting via the hydrophobic patch that surrounds the solvent-exposed His81 ligand as observed in other cupredoxins and in particular AZ (*32*−*34*). This arrangement has not previously been observed in any PAZ crystal structure and is actually slightly different from that observed for AZ. (The two molecules in the dimer are rotated relative to each other with the angle between the barrel axes and the Cu to Cu separation (12.3 Å) both less than that in AZ.) The altered packing of PAZAMI generates a different conformation of the C-terminal Asn122, which forms weak hydrogen bonds with the N^{ζ} of Lys101 via a C-terminal O atom and between its $N^{\delta 2}$ and the $O^{\epsilon 1}$ of Gln89.

Copper Site Structures. General Remarks. The geometry of a metal site in a protein is determined by a number of different factors, and it correlates with its spectroscopic and functional properties. Remarkably, significant chemical changes at a metal site can sometimes result in only subtle differences in geometry, for example, the reduction of Cu(II) to Cu(I) in a cupredoxin, which typically increases the metal ligand bond distances by as little as 0.1 Å. When comparing metal sites in proteins, it is important to know the estimated standard uncertainty (ESU) of the bond distances and angles. Table 1 shows three ESUs determined in different ways for the four structures reported in this work and refers to coordinate errors and not to bond distances or angles. To obtain the values for bond distances, one must first multiply the ESU by $3^{1/2}$ to obtain the positional error of a single atom and then by $2^{1/2}$ to take into account the error propagation for the bond distance. The ESUs of the metal−ligand bond distances based on maximum likelihood (justified because the metal site is located in a well-defined part of the protein structure) are ∼0.1 Å for the 1.30 Å structures and ∼0.3 Å for the 2.0 Å resolution structures. The ESUs of the bond distances for the 1.30 Å resolution structures are therefore in the range of the expected active site changes upon reduction of the copper ion, while the precision of the quoted bond distances in the 2.00 Å resolution structures is 3-fold lower.

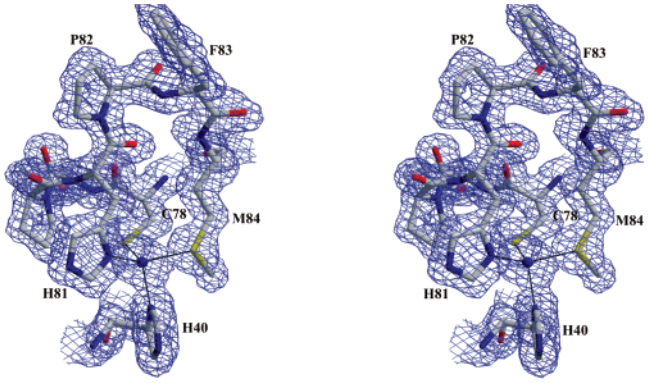

FIGURE 4: Stereoview showing a model of the Cu(II) site and the ligand-containing loop region of PAZAMI at pH 7.5 including the $2F_o-F_c$ electron density map contoured at 1.0 σ. The ligands and the mutated residues on the loop are labeled.

The precision of the structure determinations in this work has been further assessed by the analysis of two crystals of Cu(I) PAZAMI at pH 7.5. The resolution of the diffraction data for the second crystal (1.35 Å) was only slightly worse than that reported (1.30 Å) with comparable ESU values for the metal−ligand bond lengths (data not shown). The largest deviation between the individual metal−ligand bonds is 0.07 Å, which is below the precision level for these structures. This analysis demonstrates that reliable copper site geometries have been determined for the high resolution (1.30 Å) structures.

Cu(II) PAZAMI at pH 7.5. The model of the copper site of oxidized PAZAMI at pH 7.5 along with the $2F_o-F_c$ electron density map contoured at 1.0 σ is shown in Figure 4. At the resolution of this structure (1.30 Å), there are contractions in the electron density between the individual atoms and holes in the aromatic ring systems. The bond distances and angles at the distorted tetrahedral copper site are listed in Table 2. (The copper site geometry is identical in the 1.35 Å resolution structure of Cu(II) PAZAMI at this pH 7.5 (data not shown) which provides additional proof for the integrity of the Cu(II) site during data collection.) The superposition of the active sites, ligand-containing loops,

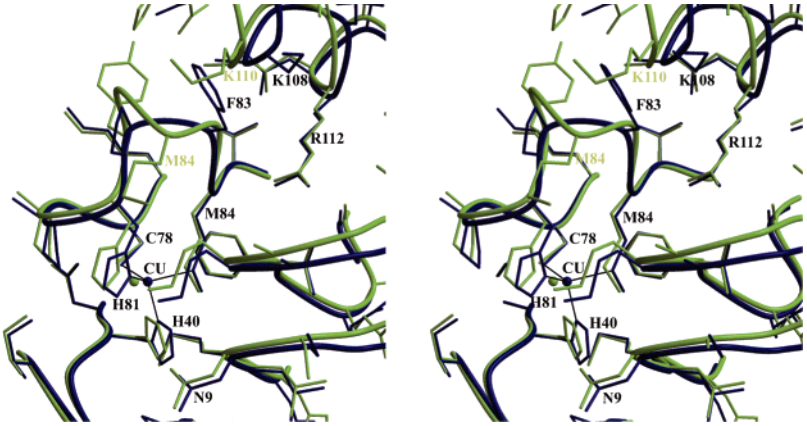

FIGURE 5: Stereoview showing an overlay of the Cu(II) sites, the C-terminal ligand-containing loops, and the adjacent regions of PAZAMI at pH 7.5 (blue) and PAZ at pH 6.0 (1BQK in green (*17*)). Important amino acids are labeled, including the ligating residues that are numbered as in PAZAMI.

Table 2: Active Site Geometry of Cu(II) and Cu(I) PAZAMI and Those of Cu(II) PAZ, AMI, AZ, and AZAMI

	Cu(II) PAZAMI pH 7.5[a]	Cu(II) PAZAMI pH 5.5[a]	Cu(I) PAZAMI pH 7.5[a]	Cu(I) PAZAMI pH 5.5[a]	Cu(II) PAZ (1 BQK)[b]	Cu(I) PAZ (1BQR)[b]	Cu(II) AMI (1AAC)[c]	Cu(II) AZAMI (2FTA)[d]	Cu(II) AZ (4AZU)[e]	Cu(II) AZ (1JZF)[f]
					Cu−ligand bond distances (Å)					
Cu−$N^{\delta 1}$(His40)	2.09	2.10	2.05	2.16	1.95	2.04	1.95	1.98	2.08	2.02
Cu−S^{γ}(Cys78)	2.22	2.27	2.10	2.14	2.13	2.19	2.11	2.14	2.24	2.21
Cu−$N^{\delta 1}$(His81)	2.09	2.24	2.50	2.64	1.92	2.11	2.03	2.09	2.01	2.08
Cu−S^{δ}(Met84)	2.39	2.38	2.37	2.43	2.71	2.85	2.90	3.29	3.15	3.32
Cu to O(Gly39)	4.41		4.50	4.62	3.94	4.04	3.92	3.19	2.97	2.60
Cu to $N^{\delta 1}{}_2S^{\gamma}$ plane	0.65	0.64	0.76	0.81	0.36	0.38	0.30	0.14	0.08	0.01
ESU[g]	0.10	0.30	0.10	0.30						
					angles (deg.)					
His40-Cu-Cys78	129	134	130	129	135	132	136	134	132	132
His40-Cu-His81	95	92	89	85	100	102	104	102	105	105
His40-Cu-Met84	90	88	95	95	87	90	85	76	77	72
Cys78-Cu-His81	108	107	101	104	114	116	113	123	123	123
Cys78-Cu-Met84	116	116	123	124	107	107	111	112	110	110
His81-Cu-Met84	118	118	117	115	107	104	100	92	87	85
Gly45-Cu-His46								79	74	80
Gly45-Cu-Cys112								97	99	97
Gly45-Cu-His117								81	89	92
Gly45-Cu-Met121								151	148	150
ϕ[h]	71	68			76		79	81	84	83

[a] Data for the PAZAMI loop-contraction variant determined in this work. The ligands listed are for PAZAMI. Gly39 is too far from the copper ion to be considered a ligand in PAZAMI (and PAZ and AMI) but is much closer to the metal in AZ and its loop-contraction variants (AZAMI shown here). [b] WT Cu(II) PAZ from *Achromobacter cycloclastes* at pH 6.0 in which the ligands are the same as those for PAZAMI except that Met86 is found in place of Met84. [c] AMI from *Paracoccus denitrificans* at pH 5−6 in which the ligands are His53, Cys92, His95, and Met98, and Pro52 is found in place of Gly39. [d] The AZAMI loop contraction variant at pH ~7 (average of all four chains) in which the ligands are His46, Cys112, His115, and Met118, and Gly45 is found in place of Gly39. [e] Cu(II) *Pseudomonas aeruginosa* AZ at pH 5.5 (average of all four chains) in which His46, Cys112, His117, and Met121 are the ligands, and Gly45 is found in place of Gly39. [f] Ru(II)(tpy)(phen)-modified AZ from *P. aeruginosa*. [g] Estimated standard uncertainty of bond distance. [h] The angle between the $N_{His}CuN_{His}$ and $S_{Cys}CuS_{Met}$ planes.

and their environments in PAZAMI and PAZ is shown in Figure 5. The hydrogen bond (see Table 3) between the $O^{\delta 1}$ of Asn9 and $N^{\epsilon 2}$ of His40, which stabilizes the position of this copper ligand, is retained in PAZAMI (the imidazole ring of His40 rotates slightly). The region between the Cys and His ligands is highly similar in the two proteins, which is not surprising given the sequence identity. Shortening the His to Met stretch and the amino acid changes in this region have a considerable effect on active site structure. However, the side chains of the Cys78 and Met84 ligands adopt positions virtually the same as those in PAZ (Cys78 and Met86). The tight turn of the introduced AMI loop between His81 and Met84, along with the rigidity imposed by the introduced Pro82, results in a slight rotation of the side chain of His81 toward the Cys and Met ligands, which pushes the copper ion further out of the plane of the three equatorial ligands (0.65 Å) than in PAZ (0.36 Å) in the direction of the axial Met ligand. This results in a shorter axial Cu−S^{δ}-(Met) bond of 2.39 Å in PAZAMI compared to that found in PAZ (2.71 Å) (*17*), AMI (2.90 Å) (*35*), AZAMI (2.95 Å) (*15*), and all other cupredoxins. The only T1 copper site with a comparably short Cu−S(Met) bond is found in the NiRs (2.45−2.49 Å) (*36*, *37*). A second axial interaction involving the backbone carbonyl oxygen of the residue adjacent to the N-terminal His ligand is found at the active site of AZ (Gly45 which neighbors His46) (*32*−*34*). The corresponding residue in PAZ is Gly39 whose backbone carbonyl is situated considerably further from the copper (3.94 Å) (*17*). The movement of the copper in PAZAMI further weakens this interaction (4.41 Å).

The superposition of the active sites of PAZAMI and AMI (*35*) is shown in Figure 6. The loop structure (which has the

Table 3: Hydrogen-Bonding Patterns around the C-terminal Ligand-Containing Loops of PAZAMI, PAZ, and AMI

atom X	atom Y	PAZAMI[a]	PAZ (1BQK)[b]	AMI (1AAC)[c]
		main-chain−main-chain[d]		
Cys78 N	Met84 O	3.0	3.0	3.2
His81 N	Cys78 O	3.3	3.2	3.1
Met84 N	His81 O	3.0	3.1[e]	2.9
Gly85 N	Tyr 82 O		3.0[e]	
Met84 N	His81 O		3.0[e]	
Tyr82 N	Cys78 O		3.0[e]	
Tyr82 N	Thr79 O		3.6[e]	
		main-chain−side-chain		
Thr79 N	Asn41 $O^{\delta 1}$	2.8	2.8	2.8
Asn41 N	Cys78 S^{γ}	3.5	3.6	3.6
His81 N	Cys78 S^{γ}	4.2	4.0	4.0
Phe83 O	Arg112 N^{η}	2.9	3.0	
Pro96 O	Arg99 $N^{\epsilon 1}$			2.7[f]
Pro96 O	Arg99 $N^{\eta 2}$			3.2[f]
		side-chain−side-chain		
Asn9 $O^{\delta 1}$	His40 $N^{\epsilon 2}$	2.8	2.8	2.7
Asn41 $N^{\delta 2}$	Thr79 $O^{\gamma 1}$	3.0	3.0	2.9
Glu43 $O^{\epsilon 2}$	Thr79 $O^{\gamma 1}$	2.7	2.8	2.7[f]

[a] Cu(II) PAZAMI at pH 7.5; this work. [b] *Achromobacter cycloclastes* Cu(II) PAZ at pH 6. [c] AMI from *Paracoccus denitrificans* at pH 5−6. [d] The residue numbering is mainly as found in PAZAMI. In PAZ Gly85, Met86, and Arg114 replace Phe83, Met84 ,and Arg112, respectively, while PAZ also has a Met residue at position 84. In AMI Glu49, Asn54, His56, Cys92, Thr93, His95, and Met98 replace Asn9, Asn41, Glu43, Cys78, Thr79, His81, and Met84, respectively. [e] Located in the longer C-terminal ligand loop of PAZ, which includes Met84 and Met86. [f] Specific to AMI, and in the case of His56 (which corresponds to Glu43 in PAZAMI), the $N^{\delta 1}$ atom is involved.

same sequence) is quite distinct in these two proteins, and this is particularly significant for the His ligand and the subsequent Pro and Phe residues. The first sizable change in the loop is found at His81 with φ/ψ backbone dihedral angles of −122°/−76° for PAZAMI compared to −132°/−108° for AMI, followed by alterations in the conformation of Pro82 (ψ is 148° in PAZAMI and 169° in AMI). Considerable differences are also observed for Phe83, with main-chain dihedrals of −96°/179° in PAZAMI and −70°/166° in AMI. The χ_1/χ_2 side chain dihedral angles of Phe83 are also quite different in PAZAMI (−53°/26°; close to the values most common for Phe residues) compared to those in AMI (51°/82°; third most frequent conformation). The main chain conformation for the Met ligand is similar, but the side chain conformation is distinct (*vide infra*). The different conformation and position of the loop in PAZAMI and AMI seems to be caused by the hydrogen-bonding pattern around Arg112 and Arg99 in PAZAMI and AMI, respectively. In PAZAMI, the $N^{\eta 1}$ atom of Arg112 forms a hydrogen bond with the backbone carbonyl oxygens of Phe83 and Met16, while the $N^{\eta 2}$ atom hydrogen bonds to the backbone carbonyl oxygen of Ala15 (see Figure 6). The first interaction generates the rotation of the copper-binding loop, and the latter two are responsible for fixing the turn in the region around residue 15 in both PAZAMI and PAZ. In AMI, which lacks the C-terminal extension of PAZAMI from which Arg112 originates, Arg99 forms two hydrogen bonds between its N^{ϵ} and $N^{\eta 1}$ atoms and the main chain carbonyl oxygen of Pro96 (see Figure 6 and Table 3), which fixes the conformation of the loop. The differences in the main chains of PAZAMI and AMI are partly responsible for the altered side chain conformations of the Phe residue on the loop. Additionally, the loop containing Met28 in AMI is sufficiently distant to allow Phe97 to adopt the observed conformation. In PAZAMI, the region containing Ala15 and Met16 is shifted toward the C-terminal ligand-containing loop with the Met16 side chain preventing Phe83 being in the same conformation as that of Phe97 in AMI. The side chain of the axial Met ligand adopts an all trans conformation at $C^{\alpha}-C^{\beta}$ (torsion angle χ_1) and $C^{\gamma}-S^{\delta}$ (χ_3) in PAZAMI, while a gauche arrangement is found in AMI (*35*). (The arrangement in PAZAMI is the same as that found in PAZ (*17*); see Figures 5 and 6.) The altered Met conformation is probably due to the position of the turn in the region around residue 15. The distance between the C^{β} of Met84 and the backbone carbonyl oxygen of Met16 would only be 2.5 Å if the side chain of Met84 adopted a gauche conformation in PAZAMI (see Figure 6). The conformation of the metal binding loop in AMI (*35*) moves the Cys92 and His95 ligands further away from the coordinating S^{δ} of the axial Met98 generating a T1 copper site with different Cu−ligand bond lengths (see Table 2).

There are significantly fewer hydrogen bonds around the active site of PAZAMI than in PAZ (see Table 3), resulting in a number similar to that found in AMI. (The AZAMI (*15*) and AZPC (*16*) loop variants possess hydrogen-bonding patterns in the vicinity of the active site loop similar to those of AMI and PC, respectively.) A particularly important hydrogen bond is that to the coordinating Cys from the backbone amide of the residue (usually Asn) adjacent to the N-terminal His ligand, which is present in PAZAMI and all other cupredoxins. There also appear to be weak interactions between the coordinating thiolate and the backbone amide of the His ligand on the loop (this interaction is slightly weaker in PAZAMI; see Table 3). The solvent structure in the vicinity of the active site is very similar in PAZAMI and PAZ and is quite different from that seen in AMI. The surface exposed His81 and its symmetry related residue are hydrogen bonded via their $N^{\epsilon 2}$ atoms to a well-defined water molecule (W16), which is located on the 2-fold crystallographic axis. PAZ (*17*) and other cupredoxins such as PC (*19*) and AZ (*32*−*34*) exhibit a similar water molecule in their oxidized forms, but this is not commonly bound to two symmetry related C-terminal His ligands. The water molecule that hydrogen bonds to the backbone carbonyl oxygen of Gly39 is slightly further from the copper in PAZAMI than in PAZ (6.4 Å compared to 6.0 Å, respectively) consistent with the movement of the metal ion away from this residue. Additionally, a water molecule hydrogen bonded to the backbone carbonyl oxygen of Pro80 is also more distant from the copper in PAZAMI than in the WT protein.

Cu(II) PAZAMI at pH 5.5. The copper site geometry of Cu(II) PAZAMI at pH 5.5 changes very little compared to that in the high pH structure (see Table 2). The only real difference is the small increase in the $Cu-N^{\delta 1}$(His81) bond distance from 2.09 Å at high pH to 2.24 Å in the low pH form, which is accompanied by an increase of the His40−Cu−Cys78 bond angle from 129° to 134°. The pH change generates a decrease of the *c* cell constant by ∼ 0.6 Å. However, this minimal increase in the density of crystal packing in this direction should have no influence on the $Cu-N^{\delta 1}$(His81) bond distance because the crystal contacts of this surface exposed ligand are mediated via water W16 to the His81 of the symmetry related neighboring molecule.

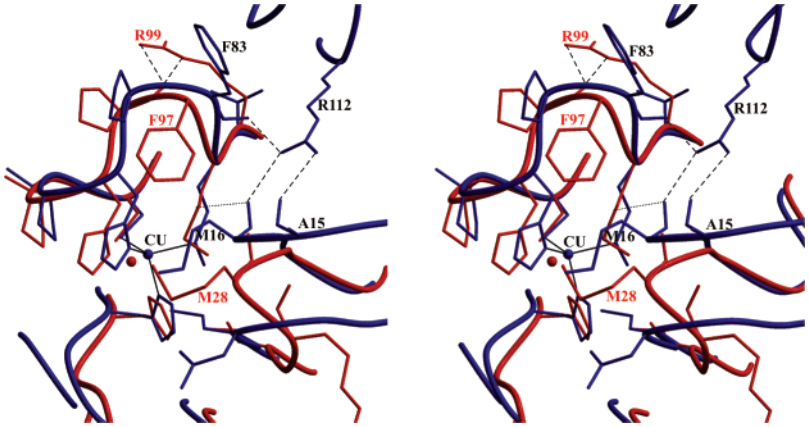

FIGURE 6: Stereoview showing an overlay of the Cu(II) sites, the C-terminal copper binding loops, and the adjacent regions of PAZAMI at pH 7.5 (blue) and AMI (1AAC in red (*35*)). A number of important amino acids in the vicinity of the active site are labeled, and certain important hydrogen bonds are displayed by dashed lines. The putative close contact between the main chain carbonyl oxygen of Met16 in PAZAMI and the C^{γ} of Met98 of AMI, which would arise if the side chain of this ligand adopted a gauche arrangement in PAZAMI, is shown as a dotted line.

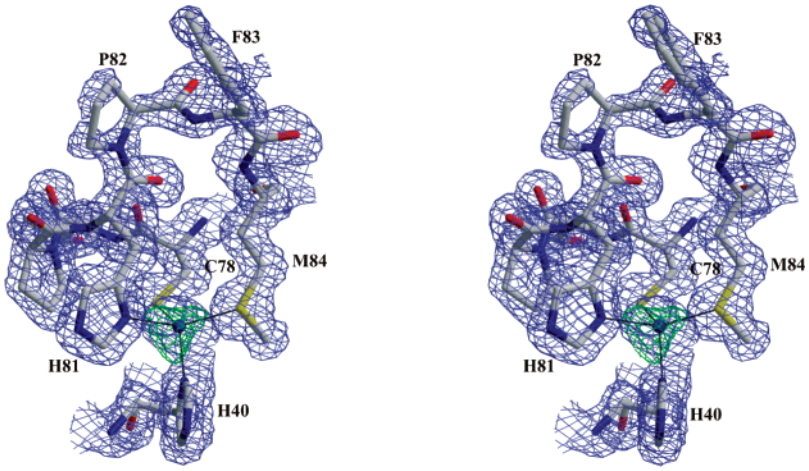

FIGURE 7: Stereoview showing a model of the Cu(I) site and the ligand-containing loop region of PAZAMI at pH 7.5 including the $2F_o-F_c$ (contoured at 1.0 σ, blue) and the F_o-F_c (contoured at -3.0 σ, green) electron densities. The ligands and the mutated residues on the loop are labeled.

Copper has not been lost from the protein as indicated by a *B*-factor in the range of those for protein atoms (see Table 1). Significant active site changes in this pH range for the Cu(II) protein would not be anticipated, and the apparent Cu$-N^{\delta 1}$(His81) bond distance increase arises from the lower precision of this structure.

Cu(I) PAZAMI at pH 7.5. The model of the copper site of Cu(I) PAZAMI at pH 7.5, along with the $2F_o- F_c$ electron density map contoured at 1.0 σ, is shown in Figure 7, and the bond distances and angles are listed in Table 2. It would be expected from the larger ionic radius of Cu(I) compared to that of Cu(II) that reduction should slightly increase the metal−ligand bond distances. In PAZAMI, the Cu$-S^{\gamma}$-(Cys78) bond decreases by 0.12 Å upon reduction, while the Cu to $N^{\delta 1}$(His81) distance increases from 2.09 Å to 2.50 Å. Careful analysis of the electron density highlights that there is residual negative difference density at the copper site (see Figure 7) and that the density between the copper ion and the imidazole ring of His81 is interrupted. This indicates that the copper site structure exists as a mixture of two forms, one with His81 protonated and dissociated from Cu(I) and the other with His81 as a ligand. The negative difference electron density at the Cu(I) site points to copper depletion, which will most probably occur in the form with His81 protonated as only three ligands remain bound to the metal. The observation of the dissociated form is consistent with a pK_a value of 6.7 for His81 determined from studies in solution on Cu(I) PAZAMI (*11*, *12*), which is close to the pH of this crystal form (the exact pH value in the crystals is difficult to determine precisely). A more flexible metal binding loop in the protonated form is identified by less well-defined electron density for the side chains of Pro82 and Phe83 in Cu(I) PAZAMI (see Figure 7). Furthermore, the water molecule hydrogen bonded to the $N^{\epsilon 2}$ atom of His81 [W16 in Cu(II) PAZAMI at pH 7.5] is less well defined in Cu(I) PAZAMI at pH 7.5 as indicated by an increase in its *B*-factor from 17 Å^2 to 34 Å^2. This can be explained by partial occupancy of this water position caused by the proportion of molecules in which the C-terminal His ligand is protonated. The water molecule that is hydrogen bonded to the main chain carbonyl oxygen of Pro80 in the Cu(II) form is found at a position that is sterically incompatible with the normal His ring position, unless the imidazole moiety is rotated by 180° about the $C^{\beta}-C^{\gamma}$ bond. The $N^{\epsilon 2}$ atom forms a hydrogen bond to this shifted water molecule and the former water molecule (W16) can no longer interact with the imidazole ring. Such a ring rotation and water structure rearrangement was first observed in reduced PC at

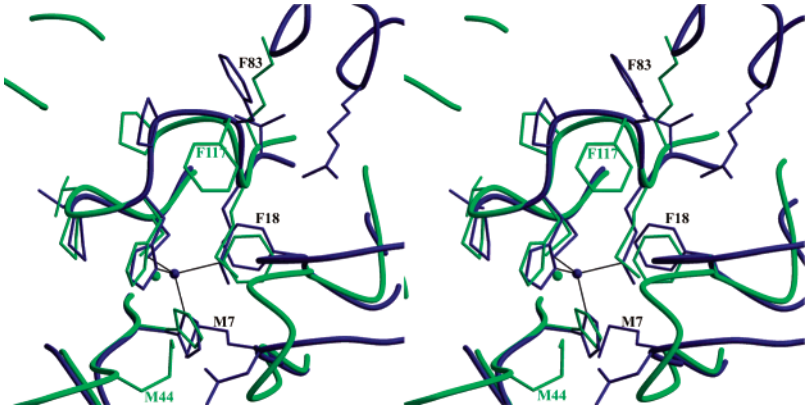

FIGURE 8: Stereoview showing an overlay of the Cu(II) sites, the C-terminal copper binding loops, and the adjacent regions of PAZAMI at pH 7.5 (blue) and AZAMI (2FTA in light green (*15*)). A number of important amino acids in the vicinity of the active site are labeled. (Some labels present in Figures 5 and 6 and the side chains of residues around Met15 of PAZAMI have been omitted for the sake of clarity.)

low pH (*19*). As the His ligand protonates, the Cu−S^{γ}-(Cys78) bond shortens to satisfy the coordination requirements of the cuprous ion. The Cu to $N^{\delta}{}_2S^{\gamma}$ plane distance is still in the range of the Cu(II) PAZAMI structures (~0.7 Å) in contrast to reduced PC at pH 3.8, where the copper is in this plane (*19*).

Cu(I) PAZAMI at pH 5.5. At this pH, the Cu to N^{δ}(His81) distance has increased to 2.64 Å, indicating that the degree of protonation is greater than that at pH 7.5. The water structure around the imidazole ring of His81 is rearranged as in Cu(I) PAZAMI at pH 7.5, and the water molecule corresponding to W16 in Cu(II) PAZAMI at pH 7.5 is even less occupied than that in the reduced structure at pH 7.5. This is further proof that the imidazole ring of His81 is protonating but that the effect is not complete, and the Cu(I) crystals were not sufficiently stable at lower pH values to allow data to be acquired. Again partial depletion of the copper has taken place in this structure as indicated by negative residual electron density at the Cu(I) site, which most probably occurs in the protonated form (see above).

DISCUSSION

Atomic resolution structures of PAZAMI have been determined by X-ray crystallography in order to understand the effect of this loop shortening experiment on the functional properties of the protein. The introduction of the short AMI loop has been compared in a number of different cupredoxin scaffolds (*11*, *12*), and the overall influence is greatest in PAZAMI. We have previously determined the structure of AZAMI as well as other loop contraction variants based on the AZ scaffold. The structures of PAZAMI determined in this study allows the influence of introducing the same AMI loop into two quite different cupredoxin folds to be assessed in molecular detail (see Figure 8).

The relative intensities of the two Cys(S) → Cu(II) LMCT bands ($A_{\sim460}/A_{\sim600}$) in the visible spectrum of PAZAMI (0.54, see Figure 2) indicates that its T1 Cu(II) site is more distorted than that of PAZ (0.45). The displacement of the copper ion from the $N^{\delta}{}_2S^{\gamma}$ plane almost doubles in PAZAMI compared to that in PAZ, which increases the lengths of the bonds to these three equatorial ligands, including the coordinating Cys, which is pivotal for the spectroscopic properties displayed by T1 copper sites (*4*, *13*, *38*, *39*). This is consistent with the greatly increased strength of the Cu−S(Met) axial interaction, resulting in the shortest bond length observed for a T1 copper site (2.39 Å), and gives rise to a more tetragonal active site structure as indicated by a 5° decrease in the dihedral angle (ϕ) between the $N_{His}CuN_{His}$ and $S_{Cys}CuS_{Met}$ planes (see Table 2). These geometric changes are in agreement with the coupled distortion model, which has been derived to explain the spectroscopic differences between distorted and classic T1 copper sites (*38*, *39*). This model assigns the differences seen in distorted T1 copper sites (those with enhanced absorption at around 460 nm and usually more rhombic EPR spectra) to an initial shortening of the Cu−S(Met) bond, which results in a tetragonal Jahn−Teller distortion involving coupled rotation of the Cys and Met ligands. It is perhaps a little surprising that the active site geometry is so different in PAZAMI as compared to PAZ considering that certain properties in particular the EPR and NMR spectra of the Cu(II) protein are on the whole very similar to those of PAZ. However, most of the directly observed hyperfine shifted resonances in the ^{1}H NMR spectra of the Cu(II) proteins are not highly sensitive to structural variations at T1 sites (*40*−*43*). It has been observed previously that the correlation between the dihedral angle ϕ and the rhombicity of the EPR spectra of T1 copper proteins is not clear-cut (*44*). Furthermore, the Met182Thr axial ligand mutation at the T1 site of *Rhodobacter sphaeroides* NiR, which influences the UV/vis spectrum, has almost no effect on the EPR properties (*45*). The loss of a strong axial ligand is compensated for by an increased Cu−S(Cys) bond in this variant, resulting in a ligand field strength similar to that in the WT protein (*46*). It should also not be overlooked that blue and green NiRs, which possess classic and distorted T1 copper sites, respectively, have very similar Cu−S(Met) bond lengths (*47*). The very short Cu−S(Met) bond in PAZAMI results from the introduction of the AMI loop into the PAZ scaffold that has to adopt a different conformation than that in AMI, which is particularly the case for the His to Met region (see Figure 6). In AZAMI, the introduced loop can be accommodated with a conformation as in AMI, and the influence on the active site structure is minimal (*15*). The comparison of the structures of PAZAMI and AZAMI demonstrates that the scaffold can influence the geometry of a metal site in a protein (see Figure 8).

An approximately 50 mV decrease in E_m is observed when the AMI loop is introduced into AZ, which results in a value almost identical to that of AMI (*12*, *15*). The introduction of the PC loop into AZ raises E_m to a value almost identical to that of PC (*16*). In these AZ chimeras, the introduced AMI and PC loops adopt conformations almost identical to those in AMI and PC, respectively (*15*, *16*). There are only limited active site structural changes in these variants, and thus the loop structure has been identified as playing an important role in tuning the E_m values of T1 copper sites, with contributions from protein dipoles in this region being the most important feature (*16*, *48*). When the AMI loop is grafted onto the PAZ scaffold, E_m is lowered by an amount similar to that in AZAMI, but the resulting value is significantly lower than that of AMI (PAZ and AMI have similar E_m values) (*11*, *12*). The structure of the AMI loop in PAZAMI is quite different from that found in AMI and AZAMI. Major differences are found for the conformations of the Pro and Phe residues in this region, the latter of which packs against the top of the long C-terminal α-helix present in PAZAMI. It would therefore be anticipated that the influence of the protein dipoles in the loop region will be different in PAZAMI as compared to that in AZAMI. The loop alterations result in a large decrease in the solvent accessibility of the Phe residue in PAZAMI compared to AMI, which is a major contributor to the lowered solvent accessibility of this region. (The loop is even less solvent accessible in AZAMI, particularly in the Cys to His section.) However, the solvent accessibility of the ligating residues is similar in PAZAMI, PAZ, AZAMI, and AMI. These comparisons are important because the thermodynamics of reduction of T1 copper sites has been found to be dominated by solvent reorganization effects (*49*). However, the solvent arrangement near the active site of PAZAMI and PAZ are similar, which is quite different from that in AMI (and AZAMI). The arrangement of solvent molecules seen close to T1 copper sites in crystal structures and the solvent accessibility of the ligating residues probably has little influence on E_m (*16*).

Other factors that can influence the E_m values of T1 copper sites are the active site structure and the hydrogen-bonding pattern in this vicinity (*50*, *51*). This latter aspect of PAZAMI is comparable to AMI and AZAMI and is quite distinct from the arrangement seen in PAZ (see Table 3). The hydrogen-bonding pattern involving the Cys ligand has been identified (*50*) as a key feature controlling E_m, which is similar in PAZAMI, AZAMI, AMI, and PAZ. Another active site property that has been predicted to influence E_m is the presence of a second weak axial interaction at the active site, trans to the Met ligand, from a backbone carbonyl oxygen atom (*50*), and this is thought to be particularly important in AZ where the oxygen atom is only ~3 Å from the copper ion (*32*−*34*). In PAZ (*17*) and AMI (*35*), the corresponding atom is ~4 Å from the metal, and because of the movement of the copper toward the axial Met ligand, the distance is even greater in PAZAMI (see Table 2). However, at this distance from the metal, this change probably has little influence. The further displacement of the copper from the $N^{\delta}{}_2S^{\gamma}$ plane toward the axial Met ligand must have an effect on E_m. The lower E_m observed for PAZAMI would indicate that the geometry changes at the active site have led to a stabilization of the Cu(II) form of the protein. The movement toward the thioether sulfur would be expected to stabilize Cu(I), but this is accompanied by an increase in the Cu−S(Cys) bond, which probably has the opposite effect. The modification from three strong equatorial ligands in PAZ toward a more tetragonal arrangement in PAZAMI would stabilize Cu(II), and it is therefore suggested that this is one of the major factors influencing E_m. The fact that the PAZAMI and AZAMI loop mutations have a similar influence on E_m seems to be purely coincidental.

The k_{ESE} value for PAZAMI is 8-fold smaller than that for PAZ at pH 7.6 (*11*, *12*). The structural studies reported here show that His81 protonation is partly observed at pH 7.5, and therefore, a possible reason for the observed decrease in intrinsic ET reactivity is an increased λ_i caused by this effect. However, studies performed in solution demonstrate that the pK_a for His81 is 6.7, which is considerably lower than the pH of the structural studies (the exact pH values in the crystals is difficult to know) (*11*, *12*). Because k_{ESE} was determined by analyzing the relaxation behavior of His ligand ^{1}H NMR resonances (including His81), whose chemical shift values are dependent on the protonation state, it is known that deprotonated His81 was mainly present in these experiments. An alternative reason for the decreased intrinsic ET reactivity is the influence of the loop mutation on the structure and properties of the hydrophobic patch that surrounds the His81 ligand, which is known to be the recognition site for ESE (*52*−*55*). The influence of loop contractions in AZ on ESE has been interpreted by their impact on the hydrophobicity in this region, which is minimal for AZAMI, resulting in a k_{ESE} value almost identical to that of AZ (*15*, *16*). The accessible nonpolar area in this region is increased from 220 Å^2 in PAZ (made up of Met16, Pro80, His81, Tyr82, Gly83, and Met84) to 260 Å^2 in PAZAMI (consisting of Met16, Pro80, His81, Pro82, and Phe83). The major effect is the introduction of the Pro and Phe residues between the His and Met ligands in PAZAMI, which have a significantly greater contribution to the hydrophobicity of this area than Tyr82 and Met84 in PAZ. The enhanced hydrophobicity is probably the reason for adjacent molecules packing via this region in the crystal lattice of PAZAMI (not seen before in any other PAZ structure) and would be expected to enhance the association constant for the PAZAMI homodimer as compared to the WT protein (*55*). However, the loss of the flexible Met side chain and particularly the Tyr in this region, which has been identified as a commonly found residue at the interfaces of proteins involved in transient interactions (*56*), could be a more significant factor.

The pK_a value for the His81 ligand in Cu(I) PAZAMI is ~2 pH units higher than that in PAZ (*57*) and almost exactly matches that for His96 in AMI (*9*, *11*, *12*, *58*). Given the altered arrangements of the loops and copper sites in PAZAMI and AMI, it would appear that the detailed structure in this region is not a main determinant of the pK_a value for the His ligand on the loop. An identical change in pK_a is seen when the AMI loop is introduced into PC (*12*). In the case of AZAMI, a pK_a value ~1 pH unit lower than that in AMI, PAZAMI, and PCAMI is observed (*12*). However, this is considerably higher than that for AZ. (A pK_a of < 2 has been estimated (*59*).) The introduction of the longer PAZ and PC loops into AMI results in decreases in the His ligand pK_a in the Cu(I) protein to match those of PAZ and PC, whereas introduction of the AZ loop has little effect (*9*, *10*,

58). Detailed thermodynamic studies of these AMI variants have identified that decreases in the pK_a have an important entropic contribution (*58*). The favored formation of the Cu(I)−N(His) bond upon lengthening the loop has been suggested as arising from increased flexibility in this region in the reduced protein (*58*). The hydrogen-bonding pattern around the active site is similar in PAZAMI, AMI (*35*), and also AZAMI (*15*), which would indicate that this feature does not influence the pK_a value. The length of the loop does affect the pK_a for the His ligand, but the structural features that regulate this effect remain unknown. The loop mutations may lead to structural alterations that influence rotational barriers involved in the dissociation and protonation of the His ligand, which can have a significant effect on the observed pK_a value (*60*).

CONCLUSIONS

When the short AMI loop is grafted onto the PAZ scaffold, it adopts a conformation distinct from that in AMI and also the related AZAMI loop contraction variant. This leads to a different active site structure for PAZAMI as compared to that for PAZ, which is more tetragonal with a very short axial Cu−S(Met) interaction and an increased Cu−S(Cys) bond. These changes give rise to an altered UV/vis spectrum and are responsible for the influence of this loop mutation on E_m. The different active site and loop structures do not seem to influence the pK_a for the His ligand on the loop because PAZAMI exhibits a value identical to that for AMI. The structures of PAZAMI demonstrate that interactions between a metal binding loop and the protein scaffold onto which it is grafted can appreciably influence active site geometry, which do not necessarily give rise to dramatically altered spectroscopy for the Cu(II) proteins. The residues on the copper binding loop have a sizable influence on transient protein interactions because they influence the nature of the important recognition patch that surrounds the exposed His ligand.

REFERENCES

1. Adman, E. T. (1991) Copper protein structures, *Adv. Protein Chem. 42*, 145−197.
2. Murphy, M. E. P., Lindley, P. F., and Adman, E. T. (1997) Structural comparison of cupredoxin domains: domain recycling to construct proteins with novel functions, *Protein Sci. 6*, 761−770.
3. Malmström, B. G., and Vänngård, T. (1960) Electron spin resonance of copper proteins and some model complexes, *J. Mol. Biol. 2*, 118−124.
4. Gray, H. B., Malmström, B. G., and Williams, R. J. P. (2000) Copper coordination in blue proteins, *J. Biol. Inorg. Chem. 5*, 551−559.
5. Ryde, U., Olsson, M. H. M., Pierloot, K., and Roos, B. O. (1996) The cupric geometry of blue copper proteins is not strained, *J. Mol. Biol. 261*, 586−596.
6. Ryde, U., Olsson, M. H. M., Roos, B. O., De Kerpel, J. O. A., and Pierloot, K. (2000) On the role of strain in blue copper proteins, *J. Biol. Inorg. Chem. 5*, 565−574.
7. Ryde, U., and Olsson, M. H. M. (2001) Structure, strain, and reorganization energy of blue copper models in the protein, *Int. J. Quantum Chem. 81*, 335−347.
8. Cascella, M., Magistrato, A., Tavernelli, I., Carloni, P., and Rothlisberger, U. (2006) Role of protein frame and solvent for the redox properties of azurin from *Pseudomonas aeruginosa*, *Proc. Natl. Acad. Sci. U.S.A. 103*, 19641−19646.
9. Dennison, C., Vijgenboom, E., Hagen, W. R., and Canters, G. W. (1996) Loop-directed mutagenesis converts amicyanin from *Thiobacillus versutus* into a novel blue copper protein, *J. Am. Chem. Soc. 118*, 7406−7407.
10. Buning, C., Canters, G. W., Comba, P., Dennison, C., Jeuken, L., Melter, M., and Sanders-Loehr, J. (2000) Loop-directed mutagenesis of the blue copper protein amicyanin from *Paracoccus versutus* and its effect on the structure and the activity of the type-1 copper site, *J. Am. Chem. Soc. 122*, 204−211.
11. Yanagisawa, S., and Dennison, C. (2003) Loop-contraction mutagenesis of a type 1 copper site, *J. Am. Chem. Soc. 125*, 4974−4975.
12. Yanagisawa, S., and Dennison, C. (2004) Loop-contraction mutagenesis of type 1 copper sites, *J. Am. Chem. Soc. 126*, 15711−15719.
13. Dennison, C. (2005) Investigating the structure and function of cupredoxins, *Coord. Chem. Rev. 249*, 3025−3054.
14. Dennison, C. (2005) Ligand and loop variations at type 1 copper sites: Influence on structure and reactivity, *Dalton Trans.* 3436−3442.
15. Li, C., Yanagisawa, S., Martins, B. M., Messerschmidt, A., Banfield, M. J., and Dennison, C. (2006) Basic requirements for a metal-binding site in a protein: The influence of loop shortening on the cupredoxin azurin, *Proc. Natl. Acad. Sci. U.S.A. 103*, 7258−7263.
16. Li, C., Banfield, M. J., and Dennison, C. (2007) Engineering copper sites in proteins: Loops confer native structures and properties to chimeric cupredoxins, *J. Am. Chem. Soc. 129*, 709−718.
17. Inoue, T., Nishio, N., Suzuki, S., Kataoka, K., Kohzuma, T., and Kai, Y. (1999) Crystal structure determinations of oxidized and reduced pseudoazurins from *Achromobacter cycloclastes*, *J. Biol. Chem. 274*, 17845−17852.
18. Freeman, H. C. (1981) In *Coordination Chemistry-21* (Laurent, J. L., Ed.) pp 29−51, Pergamon Press, Oxford, England.
19. Guss, J. M., Harrowell, P. R., Murata, M., Norris, V. A., and Freeman, H. C. (1986) Crystal structure analyses of reduced (Cu^I) poplar plastocyanin at six pH values, *J. Mol. Biol. 192*, 361−387.
20. Di, Bilio, A. J., Dennison, C., Gray, H. B., Ramirez, B. E., Sykes, A. G., and Winkler, J. R. (1998) Electron transfer in ruthenium-modified plastocyanin, *J. Am. Chem. Soc. 120*, 7551−7556.
21. Zhu, Z., Cunane, L. M., Chen, Z. W., Durley, R. C. E., Mathews, F. S., and Davidson, V. L. (1998) Molecular basis for interprotein complex-dependent effects on the redox properties of amicyanin, *Biochemistry 37*, 17128−17136.
22. Otwinowski, Z., and Minor, W. (1997) Processing of X-ray diffraction data collected in oscillation mode, *Methods Enzymol. 276*, 307−326.
23. Vagin, A., and Teplyakov, A. (1997) MOLREP: An automated program for molecular replacement, *J. Appl. Crystallogr. 30*, 1022−1025.
24. Murshudov, G. N., Vagin, A. A., and Dodson, E. J. (1997) Refinement of macromolecular structures by the maximum-likelihood method, *Acta Crystallogr., Sect. D 53*, 240−255.
25. Jones, T. A., Zou, J. Y., Cowan, S. W., and Kjeldgaard, M. (1991) Improved methods for building protein models in electron-density maps and the location of errors in these models, *Acta Crystallogr., Sect. A 47*, 110−119.
26. Potterton, E., Briggs, P., Turkenburg, M., and Dodson, E. J. (2003) A graphical user interface to the CCP4 program suite, *Acta Crystallogr., Sect. D 59*, 1131−1137.
27. Laskowski, R. A., McArthur, M. W., Moss, D. S., and Thornton, J. M. (1993) PROCHECK: a program to check the stereochemical quality of protein structures, *J. Appl. Crystallogr. 26*, 283−291.
28. Kleywegt, G. J., and Jones, T. A. (1994) A superposition, *ESRF/CCP4 Newsletter 31*, 9−14.
29. Tsodikov, O. V., Record, M. T., and Sergeev, Y. V. (2002) Novel computer program for fast exact calculation of accessible and molecular surface areas and average surface curvature *J. Comput. Chem. 23*, 600−609.
30. Esnouf, R. M. (1997) An extensively modified version of MolScript that includes greatly enhanced coloring capabilities, *J. Mol. Graphics Modell. 15*, 132−134.
31. Merritt, E. A., and Murphy, M. E. P. (1994) Raster3D version 2.0: a program for photorealistic molecular graphics, *Acta Crystallogr., Sect. D 50*, 869−873.
32. Baker, E. N. (1988) Structure of azurin from *Alcaligenes denitrificans*, *J. Mol. Biol. 203*, 1071−1095.
33. Nar, H., Messerschmidt, A., Huber, R., van de Kamp, M., and Canters, G. W. (1991) Crystal structure analysis of oxidized

Pseudomonas aeruginosa azurin at pH 5.5 and pH 9.0: A pH-induced conformational transition involves a peptide-bond flip, *J. Mol. Biol. 221*, 765−772.
34. Crane, B. R., Di Bilio, A. J., Winkler, J. R., and Gray, H. B. (2001) Electron tunneling in single crystals of *Pseudomonas aeruginosa* azurins, *J. Am. Chem. Soc. 123*, 11623−11631.
35. Cunane, L. M., Chen, Z. W., Durley, R. C. E., and Mathews, F. S. (1996) X-ray structure of the cupredoxin amicyanin from *Paracoccus denitrificans* refined at 1.31 Å resolution, *Acta Crystallogr., Sect. D 52*, 676−686.
36. Ellis, M. J., Dodd, F. E., Sawers, G., Eady, R. R., and Hasnain, S. S. (2003) Atomic resolution structures of native copper nitrite reductase from *Alcaligenes xylosoxidans* and the active site mutant Asp92Glu, *J. Mol. Biol. 328*, 429−438.
37. Antonyuk, S. V., Strange, R. W., Sawers, G., Eady, R. R., and Hasnain, S. S. (2005) Atomic resolution structures of resting-state, substrate- and product-complexed Cu-nitrite reductase provide insight into catalytic mechanism, *Proc. Natl. Acad. Sci. U.S.A. 102*, 12041−12046.
38. La Croix, L. B., Shadle, S. E., Wang, Y., Averill, B. A., Hedman, B., Hodgson, K. O., and Solomon, E. I. (1996) Electronic structure of the perturbed blue copper site in nitrite reductase: Spectroscopic properties, bonding, and implications for the entatic/rack state *J. Am. Chem. Soc. 118*, 7755−7768.
39. La Croix, L. B., Randall, D. W., Nersissian, A. M., Hoitink, C. W. G., Canters, G. W., Valentine, J. S., and Solomon, E. I. (1998) Spectroscopic and geometric variations in perturbed blue copper centers: Electronic structures of stellacyanin and cucumber basic protein, *J. Am. Chem. Soc. 120*, 9621−9631.
40. Bertini, I., Fernández, C. O., Karlsson, B. G., Leckner, J., Luchinat, C., Malmström, B. G., Nersissian, A. M., Pierattelli, R., Shipp, E., Valentine, J. S., and Vila, A. J. (2000) Structural information through NMR hyperfine shifts in blue copper proteins, *J. Am. Chem. Soc. 122*, 3701−3707.
41. Sato, K., and Dennison, C. (2002) Effect of histidine 6 protonation on the active site structure and electron-transfer capabilities of pseudoazurin from *Achromobacter cycloclastes*, *Biochemistry 41*, 120−130.
42. Donaire, A., Jiménez, B., Fernández, C. O., Pierattelli, R., Niizeki, T., Moratal, J. M., Hall, J. F., Kohzuma, T., Hasnain, S. S., and Vila, A. J. (2002) Metal-ligand interplay in blue copper proteins studied by ^{1}H NMR spectroscopy: Cu(II)-pseudoazurin and Cu(II)-rusticyanin, *J. Am. Chem. Soc. 124*, 13698−13708.
43. Sato, K., Kohzuma, T., and Dennison, C. (2003) Active-site structure and electron-transfer reactivity of plastocyanins, *J. Am. Chem. Soc. 125*, 2101−2112.
44. van Gastel, M., Boulanger, M. J., Canters, G. W., Huber, M., Murphy, M. E. P., Verbeet, M. P., and Groenen, E. J. J. (2001) A single-crystal electron paramagnetic resonance study at 95 GHz of the type 1 copper site of the green nitrite reductase of *Alcaligenes faecalis*, *J. Phys. Chem. B 105*, 2236−2243.
45. Olesen, K., Veselov, A., Zhao, Y., Wang, Y., Danner, B., Scholes, C. P., and Shapleigh, J. P. (1998) Spectroscopic, kinetic, and electrochemical characterization of heterologously expressed wild-type and mutant forms of copper-containing nitrite reductase from *Rhodobacter sphaeroides* 2.4.3, *Biochemistry 37*, 6086−6094.
46. Basumallick, L., Szilagyi, R. K., Zhao, Y., Shapleigh, J. P., Scholes, C. P., and Solomon, E. I. (2003) Spectroscopic studies of the Met182Thr mutant of nitrite reductase: Role of the axial ligand in the geometric and electronic structure of blue and green copper sites, *J. Am. Chem. Soc. 125*, 14784−14792.
47. Sato, K., and Dennison, C. (2006) Active site comparison of Co^{II} blue and green nitrite reductases, *Chem.—Eur. J. 12*, 6647−6659.
48. Olsson, M. H. M., Hong, G., and Warshel, A. (2003) Frozen density functional free energy simulations of redox proteins: Computational studies of the reduction potential of plastocyanin and rusticyanin, *J. Am. Chem. Soc. 125*, 5025−5039.
49. Battistuzzi, G., Bellei, M., Borsari, M., Canters, G. W., de Waal, E., Jeuken, L. J. C., and Sola, M. (2003) Control of metalloprotein reduction potential: Compensation phenomena in the reduction thermodynamics of blue copper proteins, *Biochemistry 42*, 9214−9220.
50. Li, H., Webb, S. P., Ivanic, J., and Jensen, J. H. (2004) Determinants of the relative reduction potentials of type-1 copper sites in proteins, *J. Am. Chem. Soc. 126*, 8010−8019.
51. Yanagisawa, S., Banfield, M. J., and Dennison, C. (2006) The role of hydrogen bonding at the active site of a cupredoxin: The Phe114Pro azurin variant, *Biochemistry 45*, 8812−8822.
52. van de Kamp, M., Floris, R., Hali, F. C., and Canters, G. W. (1990) Site-directed mutagenesis reveals that the hydrophobic patch of azurin mediates electron transfer, *J. Am. Chem. Soc. 112*, 907−908.
53. Dennison, C., and Kohzuma, T. (1999) Alkaline transition of pseudoazurin from *Achromobacter cycloclastes* studied by paramagnetic NMR and its effect on electron transfer, *Inorg. Chem. 38*, 1491−1497.
54. van Amsterdam, I. M. C., Ubbink, M., Einsle, O., Messerschmidt, A., Merli, A., Cavazzini, D., Rossi, G. L., and Canters, G. W. (2002) Dramatic modulation of electron transfer in protein complexes by crosslinking, *Nat. Struct. Biol. 9*, 48−52.
55. Sato, K., Crowley, P. B., and Dennison, C. (2005) Transient homodimer interactions studied using the electron self-exchange reaction, *J. Biol. Chem. 280*, 19281−19288.
56. Crowley, P. B., and Carrondo, M. A. (2004) The architecture of the binding site in redox protein complexes: Implications for fast dissociation, *Proteins 55*, 603−612.
57. Dennison, C., Kohzuma, T., McFarlane, W., Suzuki, S., and Sykes, A. G. (1994) Reversible active site protonation and electron-transfer properties of *Achromobacter cycloclastes* pseudoazurin: Comparisons with other type 1 copper proteins, *Chem. Commun.* 581−582.
58. Battistuzzi, G., Borsari, M., Canters, G. W., di Rocco, G., de Waal, E., Arendsen, Y., Leonardi, A., Ranieri, A., and Sola, M. (2005) Ligand loop effects on the free energy change of redox and pH-dependent equilibria in cupredoxins probed on amicyanin variants, *Biochemistry 44*, 9944−9949.
59. Jeuken, L. J. C., van Vliet, P., Verbeet, M. P., Camba, R., McEvoy, J. P., Armstrong, F. A., and Canters, G. W. (2000) Role of the surface-exposed and copper-coordinating histidine in blue copper proteins: The electron-transfer and redox-coupled ligand binding properties of His117Gly azurin, *J. Am. Chem. Soc. 122*, 12186−12194.
60. Buning, C., and Comba, P. (2000) Protonation of the copper(I) form of the blue copper proteins plastocyanin and amicyanin: a molecular dynamics study, *Eur. J. Inorg. Chem.* 1267−1273.

BI701113W